

Experimental analysis of the quasi-static and dynamic torsional behaviour of shape memory alloys

Olivier Doaré, Alessandro Sbarra, Cyril Touzé, Mohamed Ould Moussa, Ziad Moumni

▶ **To cite this version:**

Olivier Doaré, Alessandro Sbarra, Cyril Touzé, Mohamed Ould Moussa, Ziad Moumni. Experimental analysis of the quasi-static and dynamic torsional behaviour of shape memory alloys. International Journal of Solids and Structures, 2012, 49 (1), pp.32-42. 10.1016/j.ijsolstr.2011.09.009 . hal-01134805

HAL Id: hal-01134805

https://ensta-paris.hal.science/hal-01134805

Submitted on 12 Mar 2016

HAL is a multi-disciplinary open access archive for the deposit and dissemination of scientific research documents, whether they are published or not. The documents may come from teaching and research institutions in France or abroad, or from public or private research centers.

L'archive ouverte pluridisciplinaire **HAL**, est destinée au dépôt et à la diffusion de documents scientifiques de niveau recherche, publiés ou non, émanant des établissements d'enseignement et de recherche français ou étrangers, des laboratoires publics ou privés.

Experimental analysis of the quasi-static and dynamic torsional behaviour of shape memory alloys

Olivier Doaré *, Alessandro Sbarra, Cyril Touzé, Mohamed Ould Moussa, Ziad Moumni

ENSTA-Paristech, Unité de Mécanique, 91761 Palaiseau Cedex, France

This paper investigates experimentally the quasi-static and dynamic torsional behaviour of shape mem-ory alloys wires under cyclic loading. A specifically designed torsional pendulum made of a Ni–Ti wire is described. Results on the quasi-static behaviour of the wire obtained using this setup are presented, giv-ing an overall view of the damping capacity of the material as function of the amplitude of the loading (imposed torsional angle), the frequency and the temperature. The dynamical behaviour is then pre-sented through measured frequency response function between forcing angle at the top of the pendulum and the difference between top and bottom rotation angles in the vicinity of the first eigenfrequency of the wire, *i.e.* in the range [0.3 Hz, 1 Hz]. The softening-type non-linearity and its subsequent jump phe-nomenon, predicted theorically by the decrease of the effective stiffness when martensite transformation starts is clearly evidenced and analysed.

Keywords:
Shape memory alloys
Pseudo-elastic behaviour
Frequency response function
Dynamical
Quasi-static

1. Introduction

Shape memory alloys (SMA) can exhibit an unusual effect: they can recover their initial shape by simple heating after being deformed up to 8–15% (Delaey et al., 1974). This property, called shape memory effect, is used in various applications in the aerospace industry (Hartl et al., 2010a,b), and also in modern medical devices (Duerig et al., 1999; Auricchio et al., 2003). Besides, at high temperatures SMA also possess the property of pseudo-elasticity, which is the ability of a SMA to accommodate large strains due to stress-induced phase change at a constant, sufficiently high temperature and to recover its undeformed shape upon unloading. This effect is associated with stress induced austenite–martensite transformation. This behaviour occurs at a temperature above a characteristic temperature of the material, referred to as A_f (austenite finish temperature). The loading and unloading paths during this cycle do not coincide, which induces an hysteresis loop in the stress–strain relationship that is responsible of energy-dissipation. SMA are then good candidates for the design of vibration dampers, and applications in civil engineering for the mitigation of seismic-induced vibrations are already proposed (Saadat et al., 2002; Auricchio et al., 2008; Ozbulut and Hurlebaus, 2011; Carreras et al., 2011).

The potential use of such materials in vibrations damping motivated fundamental works addressing the effect of time dependence of the external solicitations. A significant amount of research works focused on the effect of coupling between phase changes and thermal exchanges (Sun and Hwang, 1993; Leo and Shield, 1993; Shaw and Kyriakides, 1995; Bruno et al., 1995; Piedboeuf et al., 1998; Bernardini and Vestroni, 2003; Bernardini and Pence, 2005; Zhang et al., 2010; Morin et al., 2011). It follows that correct modeling of the mechanical behaviour of a material must include the heat exchanges with its external environment. Models neglecting this effect are referred to as *isothermal* while models considering this effect are referred to as *non-isothermal*. Energy dissipated by these materials then depends on both characteristic times of external mechanical loading and heat dissipation (Sun and Hwang, 1993).

In addition to thermal effects, inertia effects can play an important role in the overall dynamics of the system. In that case, one has also to take into account that SMA are now part of a structure with a distributed mass, hence possessing eigenmodes and eigenfrequencies. The most simple case of such systems is an oscillator whose rigidity term shows a pseudo-elastic behaviour. In this context, some theoretical works investigated the nonlinear frequency response function of such materials. Using a simplified constitutive SMA model, Masuda and Noori (2002) studied the effect of the hysteresis loop shape on the non-linear resonant response of the oscillator. With the help of isothermal and non-isothermal models based on dissipation functions, Bernardini et al. investigated the nonlinear frequency response function of such oscillators (Bernardini and Vestroni, 2003; Lacarbonara et al., 2004; Bernardini and Rega, 2005, 2010). The main features observed are (1) a softening behaviour when forcing amplitudes are such that austenite–martensite phase transformation occurs in the material, (2) a hardening behaviour for greater amplitudes, such that complete

martensite transformation is realized in the material, (3) jump effects in the frequency response function due to these softening and hardening effects, (4) chaotic behaviour in some narrow frequency/amplitude ranges. Temporal simulations of free and forced vibrations of a shape memory alloy torsional pendulum have also been presented (Seelecke, 2002) and the effect of coupling two oscillators on the occurrence of chaos has been studied (Machado et al., 2003).

On the experimental side, fewer results can be found on the dynamic behaviour of pseudo-elastic SMA oscillators. Li and Feng have measured frequency response functions of bars under traction–compression (Feng and Li, 1996; Li and Feng, 1997). The investigated frequency range, 700–1500 Hz, was very high, so that the time for the martensitic transformation to occur in a manner similar to that observed in quasi-static tests is questionable. A slight frequency shift to lower frequencies as well as a decreasing value of peak amplitude response for increasing values of the forcing, was clearly evidenced, showing the increase of damping capacity when exciting nonlinear behaviours. However, jump phenomena have not been observed. Another experimental study has been performed by Collet et al. (2001) on flexural beams, in a frequency range around 40 Hz. Once again, a shift of the resonance frequency was observed, but jump phenomena were not found. Finally, Lammering and Schmidt (2001) investigated the frequency–response curves of a pre-strained NiTi string harmonically excited in the vicinity of its first eigenfrequency, in the range 17–19 Hz, as well as a spring-mass system composed of a stiff beam with additional masses supported by SMA springs, excited at resonance around 6 Hz. In both cases, a shift of the frequency to lower values (softening behaviour) was measured but without jump phenomena. All these experimental works suggest that the damping capacity is predominant over the nonlinearity, so that the decreasing value of the maximum vibration amplitude for increasing forcing values hides the possible occurrence of jumps. However, these experimental investigations do not consider the behaviour of the system in the frequency range that is dynamically tested, precluding from a complete view of the involved phenomena.

The aim of this work is to investigate experimentally the dynamic behaviour of SMA wires under cyclic loading at a lower frequency range, as well as giving simultaneous measurements of frequency–response curves and structural material behaviour in the frequency range of dynamical testing. More specifically, the tested frequency range is here 0.3–1 Hz, in order to better understand the link between quasi-static and dynamic measurements. For that purpose, a specifically designed torsional pendulum made of a Ni–Ti wire is considered. It is clamped upstream to a motor and downstream to an inertial load. The set-up allows for measurements of both quasi-static and dynamic responses, as the inertial load can be either blocked or left free to rotate on behalf of the user. Hence, for the same frequency range, quasi-static measurements of the behaviour as well as dynamical frequency–response curves will be measured. One of the main objective is to obtain experimental evidence of the jump effect in the frequency response function of a pseudo-elastic device, as predicted by the theoretical studies. In this paper, *dynamic* properties will always refer to a case where inertia is taken into account. One then has to deal with an oscillator (or a structure). On the other hand, *quasi-static* will refer to a case without inertia terms. This distinction is worth to mention given a general confusion around the words *quasi-static* and *dynamic*: in some litterature where inertia is not considered, these terms are employed to mark the difference between models with respect to thermo-mechanical coupling (see e.g. He and Sun, 2011; Morin et al., 2011).

The paper is organized as follows: In Section 2, the experimental setup is presented. The method used to obtain quasi-static and dynamic behaviours is then described. In Section 3, experimental results on quasi-static behaviour of the NiTi wires under test are presented and discussed. In Section 4, dynamic behaviour are addressed, as well as a linear theoretical model used to estimate some mechanical constants. In Section 5, preliminary results on the effect of room temperature are presented and briefly discussed. A conclusion finally close the article.

2. Experimental setup

A specific setup has been designed in order to perform both quasi-static and dynamic tests on SMA wires, as shown in Fig. 1. It consists of a wire of length L made of the material under test. The upper part of the wire is clamped to a torque sensor, which is attached to a brush-less servomotor. The lower part of the wire is clamped to an inertial load, which consists of a rigid bar with two added masses at its extremities. A black plate with a white point is fixed above the bar. The position of the point is tracked in real-time with the help of a firewire camera and an appropriate image processing system detailed below. This allows to record the position of the bottom end as a function of time. Finally, a ball bearing is placed at the bottom of the system to prevent undesirable out-of-plane oscillations of the wire when subjected to very large rotations.

Two types of measurements can be performed with this experimental setup. For quasi-static tests, the bottom end of the wire is maintained in a fixed position, while a rotation angle path $\alpha_c(t)$ is imposed at the top of the wire. Both torque given by the sensor and real angle of rotation given by the servomotor are then recorded to obtain the curve torque versus angle of the wire. These experiments will be discussed in Section 3.

Dynamic measurements are made possible by letting the mass free to rotate. The image of a moving white dot on a black plate is recorded with a firewire camera. Images are processed as illustrated in Fig. 2: (1) Identify a coordinate system on the plane of the black plate by associating four pixels on the image to real coordinates in the plane of the plate, (2) deform each image using a transformation defined from the reference system points of the previous step, (3) filter the image so that the white dot can be easily tracked, (4) convert the position in pixels of the white dot to a real angle position, (5) output an analog signal which voltage is proportional to the computed angle. Steps (2) to (5) are done in real time at the digital image acquisition rate (60 images/s). Finally, frequency response functions between the imposed angle of rotation $\alpha_c(t)$ (at the upper part) and the relative angle between the upper part and the lower part of the wire can then be computed. The resulting data will be discussed in Section 4.

The test specimen are 2 mm diameter polycrystalline NiTi wires with a chemical composition of 56.1% Ni, obtained from AMF-France. The density of the material is $\rho \approx 6600\ \mathrm{kg/m^3}$ and it has the following experimentally determined characteristic temperatures: $A_f \sim 24\ ^\circ\mathrm{C}$, $A_s \sim 9\ ^\circ\mathrm{C}$, $M_f \sim 13\ ^\circ\mathrm{C}$ and $M_s \sim 23\ ^\circ\mathrm{C}$. Two samples of 150 mm length, with a test length of 85 mm, referred to as "Specimen 1" and "Specimen 2" were used to perform both quasi-static and dynamic tests. The wires are prone to behaviour change and breaking due to fatigue during the cycling tests so that it was impossible to perform both exhaustive quasi-static tests and dynamic tests using the same wire. For that reason, a third wire was used to perform more systematic quasi-static tests. This wire is referred to as "Specimen 3" (S3) in the following. It has a test length of 110 mm. Except for the experiments presented in Section 5, the tests were done at room temperature of 24 °C. It has to be noted that this temperature is the minimum temperature to observe a full pseudo-elastic cycle, as it is the minimum temperature to have only the austenitic phase in absence of external stress.

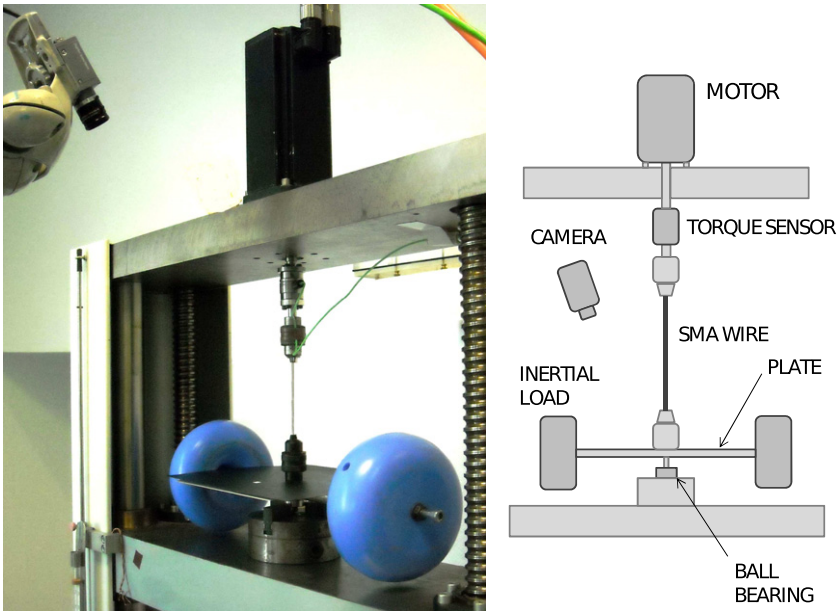


Fig. 1. (a) Photograph of the experimental setup. (b) Schematic view showing the main components.

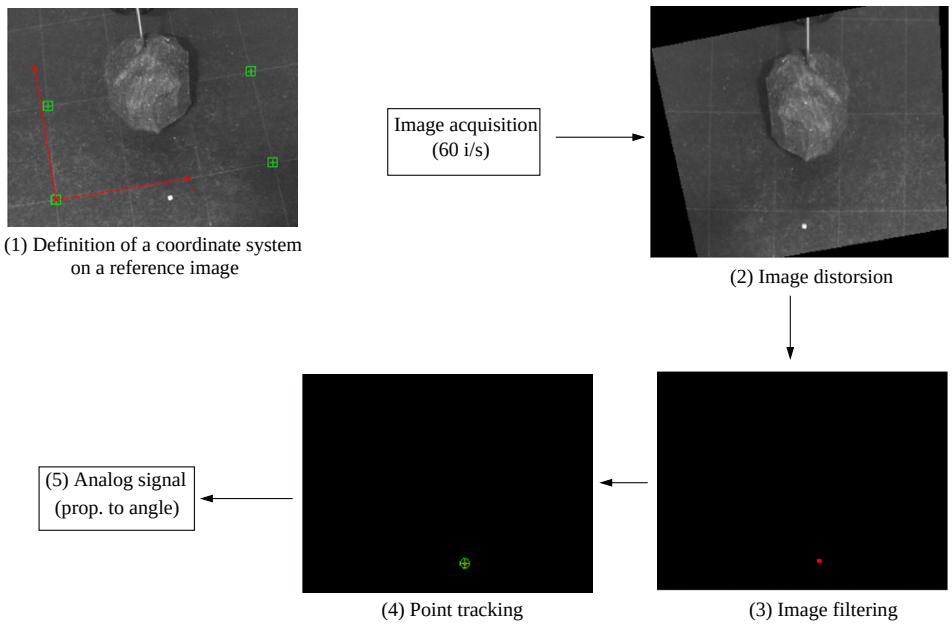


Fig. 2. Illustration of the main image processing steps to convert a image of the torsional pendulum to an analog signal proportional to the angle of rotation of the bottom end.

Finally, the rotational inertia of the system composed by the spindle, the rigid bar, the additional masses and the rotating part of the roll bearing is estimated to be

$$I_M \sim 0.02 \text{ kg m}^2. \quad (1)$$

3. Quasi-static behaviour

The objective of this section is to characterise the mechanical behaviour of the wires in torsional loading. In a first part, specimen 1 and 2 will be characterized at a fixed frequency with an evolution of the imposed angle following a triangular function. By doing this, two phenomena are neglected: the dependence on frequency, induced by the thermo-mechanical coupling (He and Sun, 2011), and the fatigue of the material that modifies its properties after a many cycles (Predki et al., 2006). However, it will be considered that this characterisation is sufficient to predict general features of the damping capacity of specimens 1 and 2. Moreover, as the dynamic tests presented in Section 4 involved many cycles, the above mentioned fatigue effects prevented us from doing both exhaustive quasi-static tests (multiple frequencies, forcing paths, forcing amplitudes) and exhaustive dynamic tests. In order to keep the properties of one same specimen almost constant for all measurements, it was then chosen to perform only basic quasi-static tests with S1 and S2, before using them in dynamic tests, and perform exhaustive quasi-static test with S3.

Let us first describe the experiments conducted on S1 and S2. It consists in quasi-static tests in which the forcing angle is a triangular function of time, at 0.01 Hz. The typical evolution of the angle and torque versus time is plotted in Fig. 3 for specimen 1 and three amplitudes of forcing: 100° (Fig. 3a), 350° (Fig. 3c) and 450° (Fig. 3e). The non-linear nature of the torque as function of the angle clearly appears on these plots. The corresponding torque versus angle relations are plotted in Fig. 3b, d and f. It has to be noted that the torque versus angle relationship is related not only to the material properties of the wire but also to the geometry, which induces a non-uniform distribution of stress and strain. As a consequence of this, one can observe that up to the maximum imposed angle at the top of the wire (450°) the completed martensitic transformation accompanied by the return to an elastic behaviour is not found. This can be easily explained by the kinematics of the torsion on a given section, where the shear strain tends to zero with the

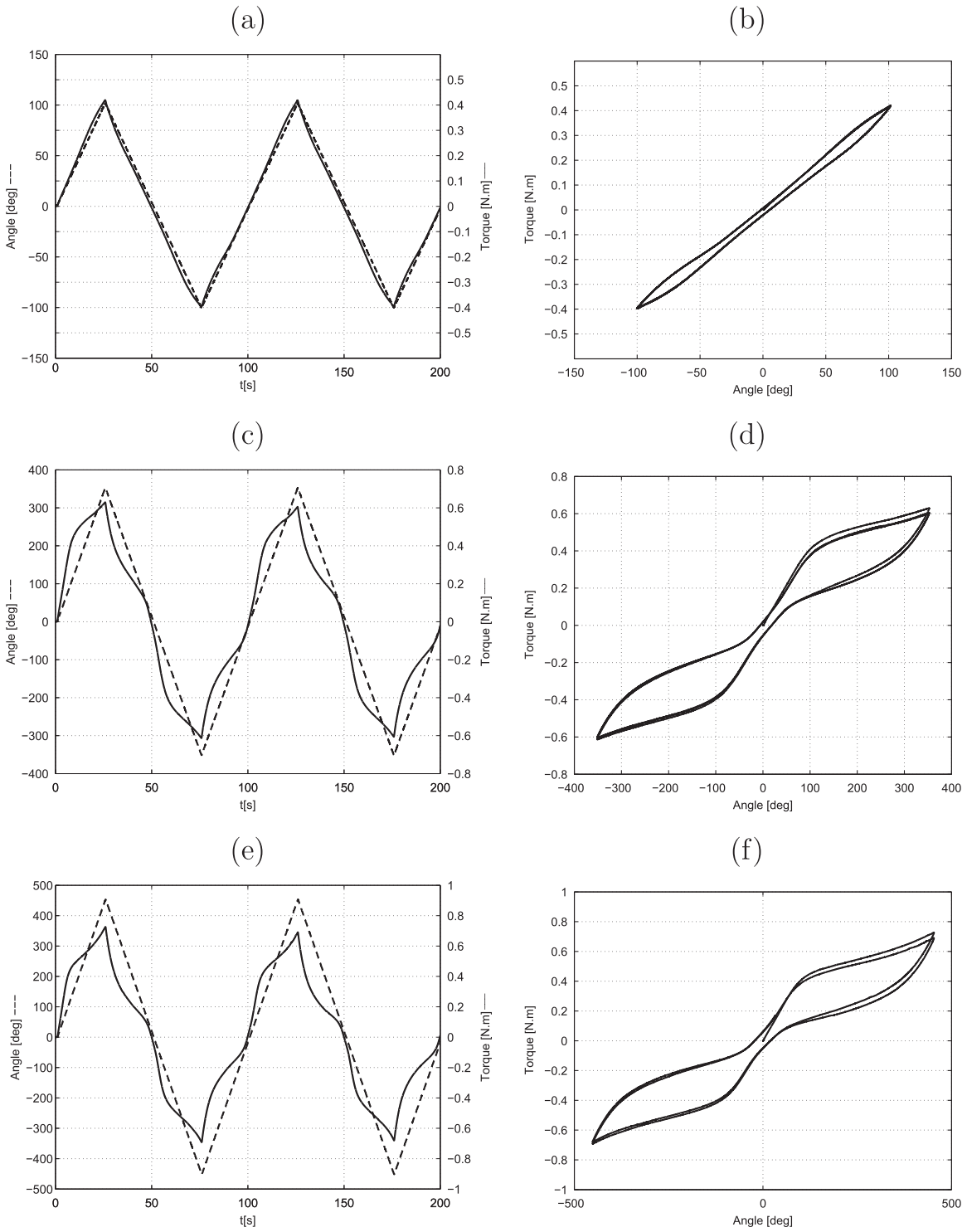


Fig. 3. Specimen 1 at room temperature (24 °C): Angle imposed at the upper clamp (– –) and torque (—-) versus time for three amplitudes of forcing: (a) 100°; (c) 350°; (e) 450°. Corresponding torque versus angle plots are presented in (b), (d), (f).

inner radius r. Hence, in the vicinity of the centre, austenite phase persists so that the obtention of a fully volumic martensitic wire can be observed only asymptotically for an imposed angle going to infinity. Conversely, in the case of a tensile test, or if a thin-walled tube was used in the torsion experiment, transformation end could be observed easily.

One can observe that the starting point of the torque angle curves deviates upon cycling. This could be the consequence of a cooling phenomenon due to latent heat absorption in reverse phase transformation, as proposed by He and Sun (2011) or due to the accumulation of slip deformations as well as residual martensite which induce residual angle (Morin et al., 2011).

The cycle shapes of specimens 1 and 2 are now compared in Fig. 4. It appears that phase transformation occurs slightly below 100° for S1, while it occurs slightly above for S2. Secondly, the area of the hysteresis loop for S1 is more important than that of S2. The angle-torque relationships of specimen 1 and 2 at 450° of forcing are plotted in Fig. 5(a) for a qualitative comparison. More quantitatively, in Fig. 5(b) the area of the loops is plotted against the amplitude angle for these two specimens. This quantity has the dimension of an energy and readily gives the energy dissipated

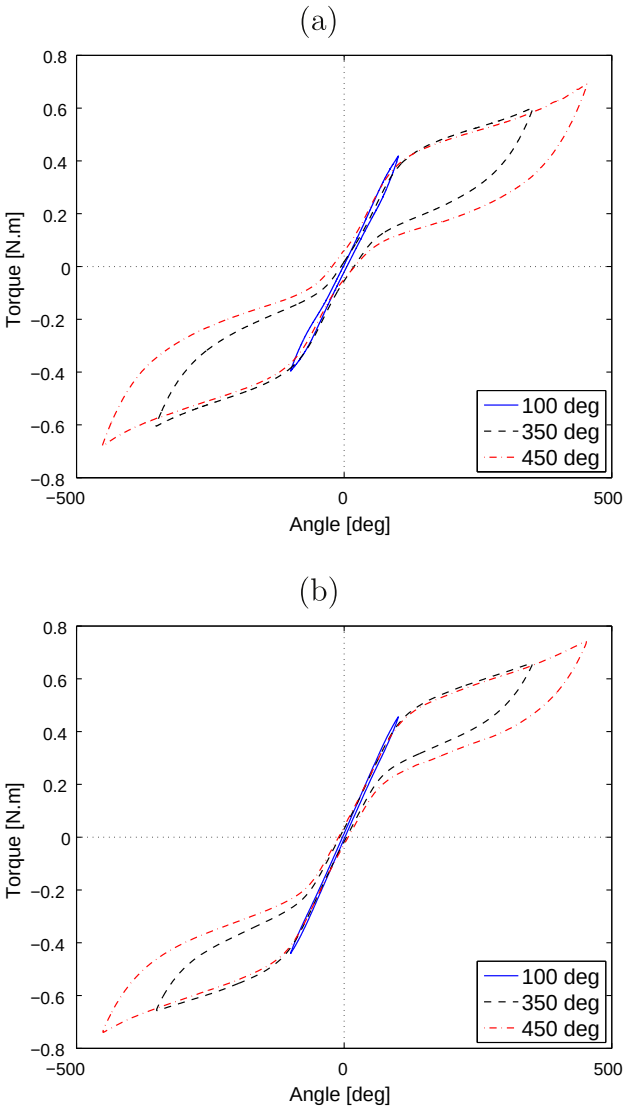


Fig. 4. Quasi-static tests: Torque versus angle of torsion for specimen 1(a) and 2(b) at three different amplitudes (100°, 350° and 450°), at room temperature (24 °C).

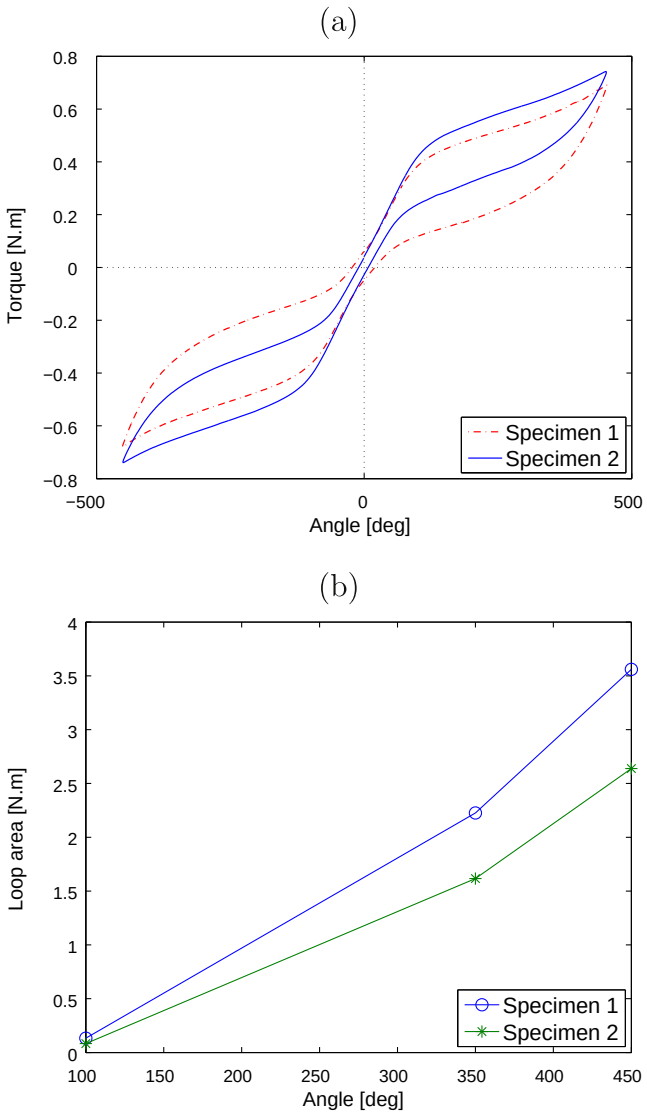


Fig. 5. (a) Comparison of the shape of hysteresis loops of S1 and S2, at an amplitude of 450° and a frequency of 0.01 Hz and (b) loop area as function of the forcing amplitude.

by the material during one cycle. It then appears that the damping capacity of S1 is superior to that of S2.

To address the dependence of the mechanical behaviour of the NiTi wires as function of the forcing characteristic time, a third specimen has been specifically used. In order to get more realistic excitations with respect to the dynamic approach, we now consider sinusoidal forcing. The wire has then been systematically stressed at frequencies between 10^{-5} Hz and 1 Hz for four different amplitudes, 175°, 250°, 350° and 450°. The hysteresis loops are compared in Fig. 6 for 175° and 450°. It appears that the increase of the cycling frequency has for effect to increase the slope of the path in the phase-transformation regime and to modify the area of the hysteresis loop. This is clearly visible on the plot at 450°, Fig. 6(b).

In order to get a more quantitative description of the damping capacity as function of the forcing frequency, the area of the hysteresis loop is plotted as function of the frequency in Fig. 7(a). The energy dissipated presents a maximum at a value of $\sim 10^{-3}$ Hz, it seems to attain a constant value at low frequencies, and it decreases monotonically at high frequencies. This particular non-monotonic evolution of the loop area as function of the frequency was already

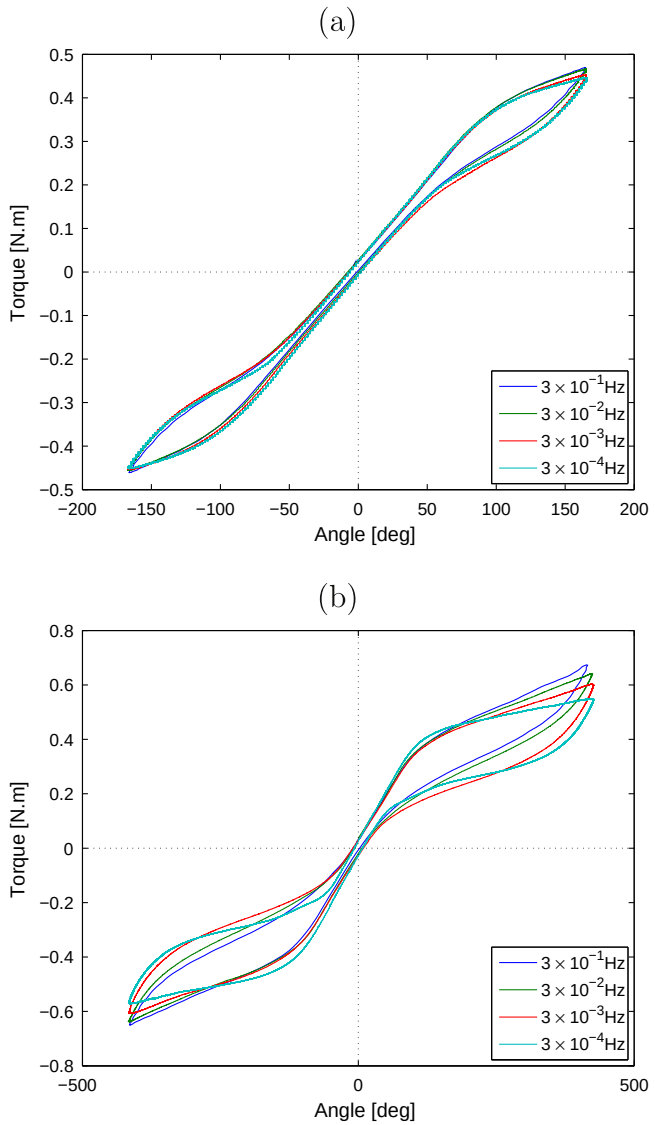


Fig. 6. Characterisation of the effect of cycling frequency, comparison of hysteresis loops at different frequencies for an amplitude of forcing of 175° and 450°.

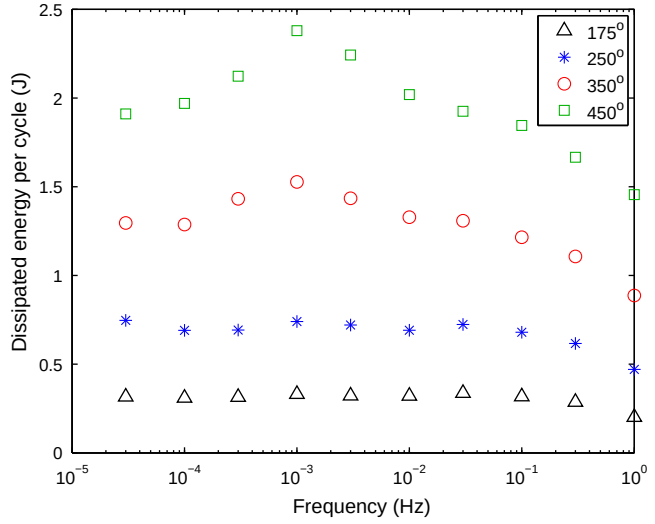


Fig. 7. Area of the hysteresis loop as function of the cycling frequency for different amplitudes of forcing.

observed experimentally in NiTi SMA under traction (Piedboeuf et al., 1998; He and Sun, 2011; Morin et al., 2011). It can be interpreted as the consequence of three different thermal effects (He and Sun, 2010). The first one is an accumulated heat due to mechanical dissipation. The second one is a latent heat effect during forward and backward phase transformations, which induces oscillations of the temperature. The last one is the heat exchange between the material and the surrounding fluid. Each of these effects occurs on different characteristic timescales and consequently, the time dependence of the material's temperature strongly depend on the forcing frequency. Finally, as the critical values of phase transformation stresses strongly depend on the temperature, the hysteresis loop shape and area also depend on the frequency. Hence, it appears that the damping effect of the material significantly depends on the frequency of forcing. This effect has to be taken into account in the context of damping of vibrations when using such materials. In our particular system, the ratio between maximum hysteresis loop area at 10^{-3} Hz and the minimum at 1 Hz is approximately equal to 1.5 at any of the four forcing amplitudes. In other words the maximum damping capacity around 10^{-3} Hz, is 50% higher than that at 1 Hz. However, if we restrict the frequency range to that explored in the dynamic analysis of the next section ([0.3 Hz, 0.8 Hz]), the maximum area is only 10–15% higher than the minimum area.

From the experimental linear behaviour at low forcing amplitudes described above, it is possible to estimate the value of the torsional spring constant of the wires, noted K. The slope of the linear path at the beginning of the first cycle before the beginning of the martensitic phase transformation is used (see Fig. 3). The shear elastic modulus G of the material in the austenitic phase is readily obtained using,

$$G = \frac{KL}{J_w}, \tag{2}$$

where J_w is the polar moment of inertia of the cross section, defined as $J_w = \frac{\pi}{2} r_w^4$, and L is the length of the wire. The resulting values of the shear modulus of the wire are reported in Table 1. These values are similar to those found in another work on the torsional behaviour of NiTi (Predki et al., 2006).

4. Dynamic behaviour of a SMA torsional pendulum

This section is devoted to the experimental study of the dynamical response of the torsional pendulum. The focus is on measuring linear and non-linear frequency response functions of the pendulum. Before addressing the experimental part, a linear model of the system is derived. It allows for the estimation of various quantities of the system, such as the moment of inertia of the inertial load and the damping induced by the ball bearing.

4.1. Single degree of freedom model of an elastic wire with a heavy lumped mass at the bottom end

A wire of length L, made of a linear elastic material of density ρ and shear modulus G, clamped at its top end denoted by $x = 0$, and having a lumped mass at its bottom $x = L$, is considered (see Fig. 8).

Table 1
Values of the shear moduli of the three specimen, estimated from experimental data.

Specimen	G (GPa)
S1	14.6
S2	15.2
S3	15.6

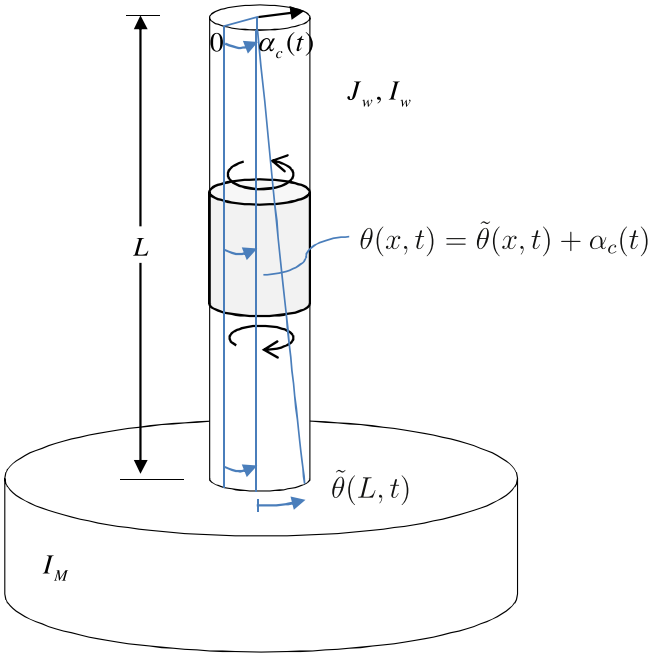


Fig. 8. Schematic view of the torsional pendulum under consideration, indicating all the notations used in the paper.

The angle of rotation of a section at a given location x is noted $\theta(x,t)$. The moment of inertia of the section is noted J_w, while its inertia is noted I_w. The rotation inertia of the lumped mass is denoted by I_M. The equation of motion for the rotation angle $\theta(x,t)$ for this system without damping and external forcing, reads (Meirovitch, 2001):

$$\frac{\partial^2\theta}{\partial t^2} - c^2\frac{\partial^2\theta}{\partial x^2} = 0, \tag{3}$$

where c is the propagation speed of torsional waves in the wire, $c = \sqrt{G/\rho}$. The boundary conditions of the present problem are,

$$\theta(0,t) = 0, \tag{4}$$

$$GJ_w\frac{\partial\theta}{\partial x}\bigg|_{(L,t)} + I_M\frac{\partial^2\theta}{\partial t^2}\bigg|_{(L,t)} = 0. \tag{5}$$

The second equation expresses the equilibrium of the momentum at $x = L$. Looking for solutions in the form $\theta(x,t) = \phi(x)e^{i\omega t}$, eigenmodes and eigenfrequencies of the problem are found after a straightforward calculation and read,

$$\phi_n(x) = B_n\sin(k_n x), \tag{6}$$

$$\omega_n = k_n c, \tag{7}$$

where k_n satisfies the following characteristic equation,

$$k_n L\tan(k_n L) = \frac{I_w}{I_M}. \tag{8}$$

Finally, B_n is chosen according to the following normalisation rule,

$$\int_0^L \phi_n^2\,dx = 1. \tag{9}$$

Eigenmodes are plotted in Fig. 9 for two different values of the ratio I_w/I_M:0.1 and 100. The second case corresponds to a very small value of the added inertia at the bottom, so that the eigenmodes are very close to the sine functions obtained in the case of a free end: $I_M = 0$.

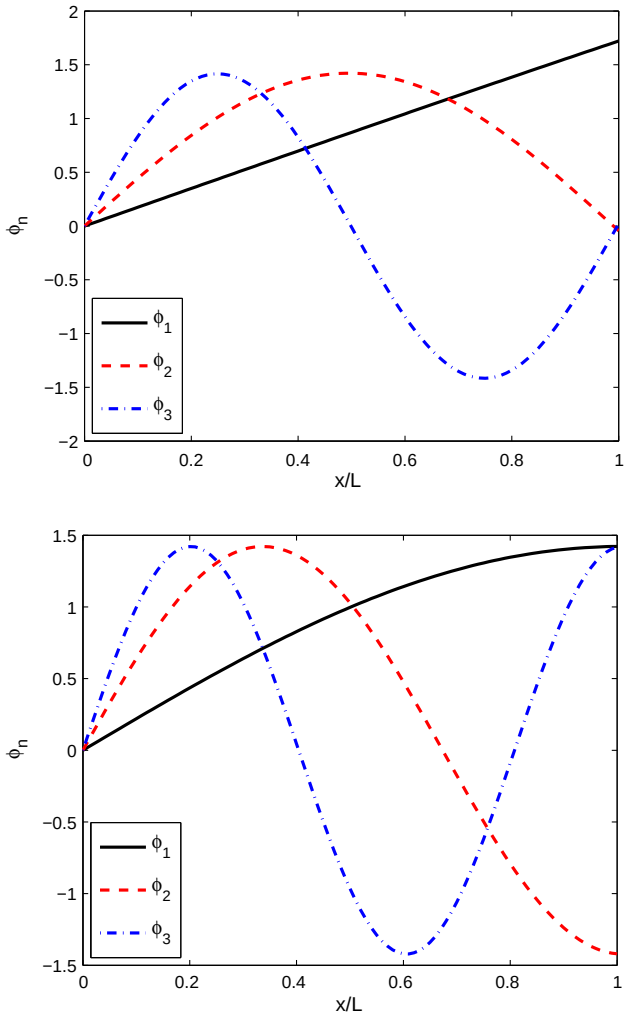


Fig. 9. First three eigenmodes of the torsional pendulum system for: (a) $I_w/I_M = 0.1$ and (b) $I_w/I_M = 100$. In the first case, the first eigenmode is almost linear, and the internal stresses and strains can be considered homogeneous along the wire.

On the other hand, for large values of I_M, the first eigenmode can be approximated by a linear function, so that torsional strain $\frac{\partial\theta}{\partial x}$ can be considered constant in each section of the wire. Moreover as I_w/I_M is small, the eigenfrequencies obey the following rule,

$$\omega_1 \simeq \frac{c}{L}\sqrt{\frac{I_w}{I_M}}, \quad \omega_n \simeq \frac{cn\pi}{L} \quad \text{for } n > 1. \tag{10}$$

This has for consequence that $\omega_1 \ll \omega_{n,n>1}$: the first eigenfrequency is set well apart from the other ones, so that the assumption of a single-mode vibration when the system vibrates in the vicinity of ω_1 is fulfilled. Another consequence of the high mass ratio value is that phase transformations occurs homogeneously along the length of the wire, due to the fact that the eigenmode is approximately a linear function.

Let us now consider the forced problem where the upper part of the wire is now assumed to rotate. The boundary condition at $x = 0$ is now,

$$\theta(0,t) = \alpha_c(t), \tag{11}$$

where $\alpha_c(t)$ represents the angle imposed by the motor (external command). Introducing the relative angle $\tilde{\theta}(x,t) = \theta(x,t) - \alpha_c(t)$, the equation of motion and its boundary conditions read,

$$\frac{\partial^2\tilde{\theta}}{\partial t^2} - c^2\frac{\partial^2\tilde{\theta}}{\partial x^2} = \frac{\partial^2\alpha_c}{\partial t^2}, \tag{12}$$

$$\tilde{\theta}(0,t) = 0, \tag{13}$$

$$GJ_w\frac{\partial\tilde{\theta}(L,t)}{\partial x} = -I_M\frac{\partial^2\tilde{\theta}(L,t)}{\partial t^2} - I_M\frac{\partial^2\alpha_c}{\partial t^2}. \tag{14}$$

A modal projection is assumed by expanding the unknown as $\tilde{\theta} = \sum_n q_n(t)\phi_n(x)$. The orthogonality of eigenmodes along with the peculiar treatment for problem with a lumped mass at the boundary (Meirovitch, 2001), allows derivation of the forced mass-spring oscillator equation for each modal amplitude q_n. Assuming also modal damping, it reads,

$$\ddot{q}_n + 2\zeta_n\omega_n\dot{q}_n + \omega_n^2 q_n = -\frac{1}{m_n}F_n\frac{\partial^2\alpha_c}{\partial t^2}, \tag{15}$$

where

$$F_n = -\int_0^L \rho\phi_n(x)dx - \frac{I_M}{J_w}\phi_n(L), \tag{16}$$

$$m_n = \int_0^L \rho\phi_n(x)^2\,dx + \phi_n^2(L)\frac{I_M}{J_w}, \tag{17}$$

$$k_n = \int_0^L G\phi_n'(x)^2\,dx, \tag{18}$$

and $\omega_n^2 = k_n/m_n$. In the experiment, we will assume that only the first mode is excited so that q_n=0 for $n > 1$. The non-dimensional damping parameter $\zeta = \zeta_1$ is evaluated empirically from experiments at low amplitudes of forcing so that this parameter is supposed to model all damping effects except that brought by the non-linear behaviour of the SMA and the occurence of the hysteresis loop.

4.2. Experimental linear dynamic behaviour of SMA wires

A first set of dynamic experiments has been performed at low values of forcing amplitude in order to ensure a linear response. It allows for measurements of the first eigenfrequency, as well as to estimate the only parameter that is left unknown in the linear model derived above: the non-dimensional modal damping parameter. Measurements are realized by letting the added mass free to oscillate. The imposed angle at the top of the wire corresponds now to a harmonic excitation of amplitude α_c and frequency f_c: $\alpha_c(t) = \alpha_c\cos 2\pi f_c\, t$. The frequency response function of $\tilde{\theta}$ is plotted in Fig. 10(a) for three forcing angles $\alpha_c = 0.2°$, 0.3°, 0.5°. The theoretical frequency response function is also plotted, with a modal damping adjusted so that the amplitude of the resonance peak is the same as the experimental one. The resulting value of the modal damping is plotted in Fig. 10(b).

Two main observations are drawn from these linear measurements. Firstly, one can notice a very slight decrease of the measured resonant frequency with increasing α. This behaviour is not attributed to the material since for such amplitudes of oscillations, the quasi-static response is measured to be linear. It is assumed that it comes from the rolling bearing placed at the bottom end of the experimental set-up. The lubricated part of the ball bearing effectively ensures non-linear behaviour for small amplitude values. As observed in Fig. 10b, the fitted linear value tends to a constant value, which shows that the non linear effects of the ball bearing only plays a role at small amplitudes.

4.3. Non-linear oscillations of SMA wires

In this section, frequency–response functions (FRFs) for the two tested specimens S1 and S2 are presented. A step-by-step procedure for increasing and decreasing values of the excitation

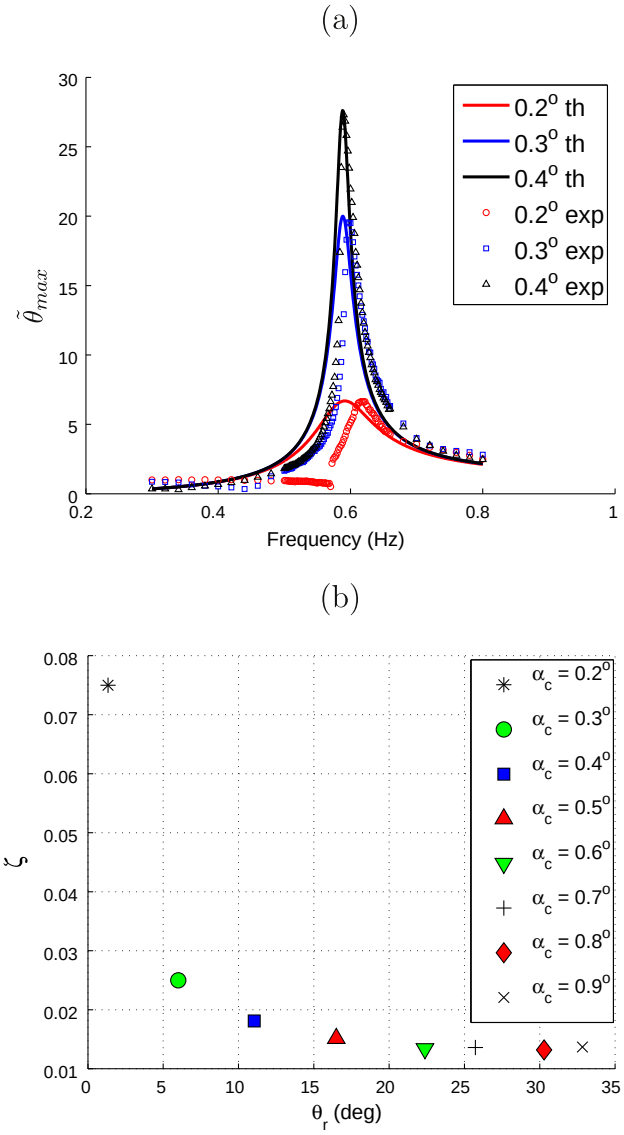


Fig. 10. (a) Experimental normalised frequency response function for three values of α_c compared with the theoretical response function where the damping parameter is adjusted and (b) damping parameter as function of response amplitude.

frequency f_c is necessary in order to obtain all the solution branches in the non-linear regime. For each frequency f_c, a settle time of 30 s is awaited so that the transient dies away, then a measurement time of 20 s is recorded during the steady-state regime, from which the maximum value of the relative rotation $\tilde{\theta}$ is extracted. Hence 50 s are necessary for each measured points. The frequency spacing is fixed to 0.02 Hz away from resonance, and is decreased to 0.001 Hz in the vicinity of critical points in order to avoid loss of the stable branches too quickly, as it is well known that their basin of attraction severely shrinks when approaching the jump points. These settings result in a measurement time of approximately four hours for obtaining a complete frequency–response curve for a given amplitude α_c (two hours for increasing values of f_c, 2 h for decreasing values).

Fig. 11 shows the measurements obtained for specimen S1, and for $\alpha_c = 0.5°$, 2°, 8° and 15°. For $\alpha_c = 0.5°$, a linear response is obtained, as already shown in the precedent section. For $\alpha_c = 2°$, the amplitude of the response attains 60°, and for that value a very small loop begins to form in the measured behaviour, resulting in a nonlinear response in the FRF. The softening behaviour is

already noticeable with a slight decrease of the resonant frequency, while a small jump phenomenon at the end of stable branches is seen. This observations are strengthened for $\alpha_c = 8°$ and 15°. For these values, amplitude responses go above 100° so that the martensitic transformation more clearly sets in, resulting in a very clear softening measured behaviour accompanied by a jump phenomenon at the end of stable branches. It has also been observed that the transients were significantly longer when jumping from the main branch obtained for decreasing frequencies and giving rise to the larger amplitude responses, resulting in the points observed around 0.55 Hz for $\alpha_c = 2°$, 0.48 Hz for $\alpha_c = 8°$, and 0.44 Hz for $\alpha_c = 15°$.

Fig. 12 shows the FRFs obtained for specimen S2, and for the same amplitudes of forcing. The most salient features are comparable to those found for S1. A slight nonlinear behaviour is found for $\alpha_c = 2°$, whereas it is enhanced for $\alpha_c = 8°$ and 15° with a clear appearance of jump phenomena. The main difference with S1 resides in the fact that, for the same levels of forcing amplitudes, measured responses show larger magnitudes. This is a direct consequence of the damping capacity of the two specimens already noticed in Fig. 5. The area of the hysteresis loop of S2 being smaller than that of S1, its capacity to damp vibrations is less important, so that the peak amplitudes obtained at resonances in FRFs are more important for S2.

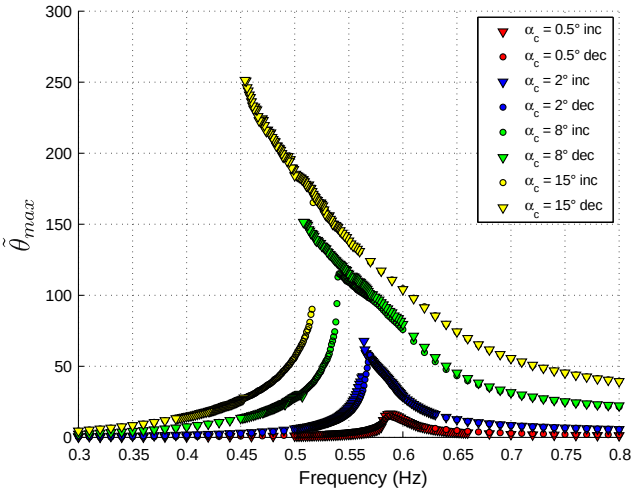


Fig. 12. Frequency–response functions (FRFs) for specimen S2, for increasing values of the forcing amplitude: $\alpha_c = 0.5°$, 2°, 8° and 15°. Measured responses for increasing values of f_c are marked by circles, and by triangles for decreasing values.

5. Temperature effect

A preliminary study of the effect of temperature is now presented. Quasi-static and dynamic measurements at 65 °C have been performed. The temperature is imposed by blowing hot air on the wire. The main objective is to address the effect of a change in the quasi-static behaviour of the material on the FRFs of the oscillator. Results of quasi-static measurements at 24 °C and 65 °C performed on specimen S2 with a triangular forcing at a frequency of 0.01 Hz are plotted in Fig. 13. Firstly, a significant increase of the slope of the torque during the first part of the first cycle is observed. This indicates that the shear elastic modulus G of the austenitic phase increases with increasing temperature. The estimated value from these data is $G \sim 20.3$ GPa, a higher value than the one referenced in Table 1. Secondly, the area of the hysteresis loop is much larger at high temperatures than at room temperature. Measured shape areas for these two experiments are 2.5 J and 5 J at 24 °C and 65 °C respectively. The wire has hence an increased damping capacity at 65 °C. Thirdly, the shape of the loop clearly indicates that cooling due to latent heat absorption and residual strain occurs during the cycle, as already discussed in Section 3.

It is expected that the change in the quasi-static behaviour will influence the dynamic behaviour in two ways: (1) the linear eigenfrequency will increase, due to the increased shear elastic modulus of the material and (2) the amplitude of the response at nonlinear resonance will decrease, due to the increase of the energy dissipated per cycle of oscillation. These predictions are indeed verified on the frequency response functions at 65 °C, plotted in Fig. 14: At

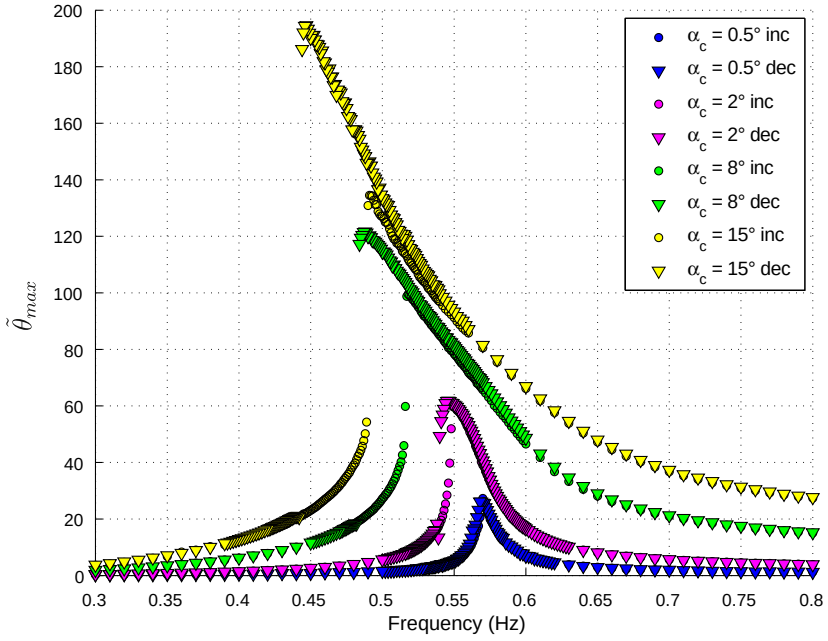


Fig. 11. Frequency–response functions (FRFs) for specimen S1, for increasing values of the forcing amplitude: $\alpha_c = 0.5°$, 2°, 8° and 15°. Measured responses for increasing values of f_c are marked by circles, and by triangles for decreasing values.

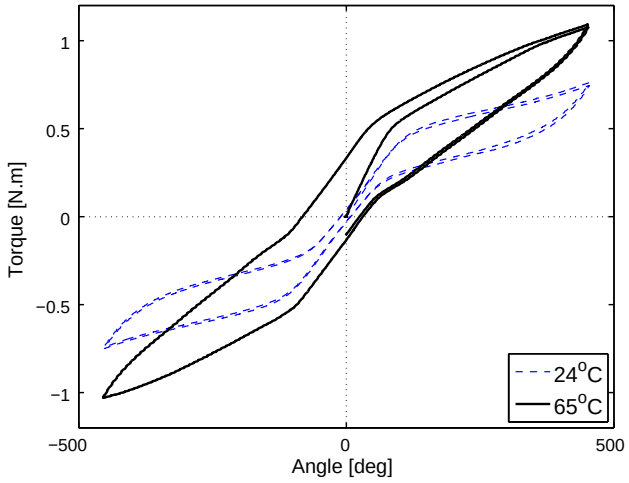


Fig. 13. Torque versus angle of torsion for specimen 2 forced at 450 degrees amplitude, 0.01 Hz frequency at 65 °C (bold line) compared with the same data at 24 °C (dashed line).

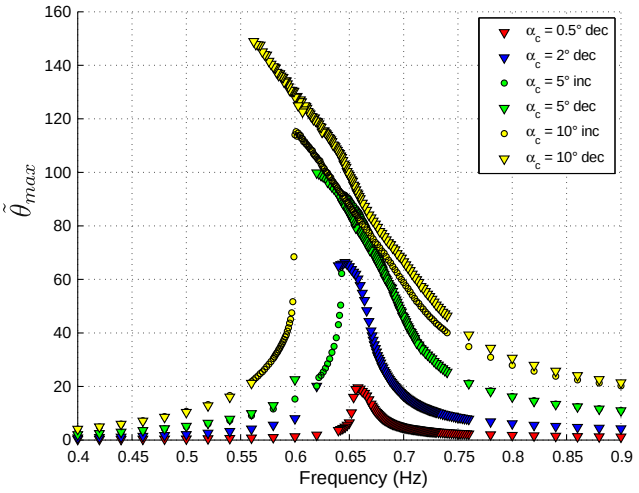


Fig. 14. Frequency response function of specimen 2 at a temperature of 65 °C.

65 °C, the linear resonance frequency attained at a low forcing amplitude of 0.5°, is approximately 0.67 Hz, a larger value than 0.58 Hz, obtained at 24 °C. When increasing the forcing amplitude, the softening behaviour described in the previous section, as well as the associated jump effect are again observed. The amplitudes attained for an equivalent value the forcing amplitude are lower at high temperature, due to the increased damping capacity of the material.

6. Discussion

Shape-memory alloys featuring pseudo-elastic behaviour are attractive candidates to damp undesirable vibrations as they efficiently convert mechanical energy into thermal energy. Understanding the impact of the hysteretic behaviour of the devices on the response of the forced oscillators is an essential element to assess the potential performance of such systems. Hence, the present article investigated experimentally the quasi-static and dynamic torsional behaviour of a NiTi wire.

Quasi-static mechanical behaviour has been characterized through the measurement of the non-linear torsional angle/torque relationship at different frequencies, amplitudes and temperatures. As in many other studies an hysteresis loop has been clearly observed and its area, which quantify its damping capacity, has been observed to depend on all these parameters. A maximum damping capacity has been observed around 10^{-3} Hz, which is in the line of previous studies on shape memory alloys (He and Sun, 2011; Morin et al., 2011). However, these works were mainly focused on traction–compression behaviour while our work dealt with torsional behaviour.

The dynamic behaviour has then been addressed by measuring the frequency response function of a torsional pendulum which torsion spring element is the NiTi wire previously characterized. Most of the features predicted by theoretical studies have been observed in the present work: softening effect of the non-linearity, jumps in the amplitude of the response associated to this softening effect and non-linear damping effect of the SMA.

On the experimental side, natural extensions to this work include a more precise characterisation of the temperature dependence, the characterisation of internal loops in the quasi-static behaviour and the study of the fatigue of the dynamically loaded material. Additionally, experiments with different thermal conductivities for the surrounding fluid may be considered. For instance, putting the wire in water increases the heat transfer and increases the damping capacity of the material. On the numerical side, it is worth investigating the non-linear extension of the linear model presented in this paper is worth investigating. Subsequent work will be focused on these extensions to this experimental analysis.

References

Auricchio, F., Fugazza, D., Desroches, R., 2008. Rate-dependent thermo-mechanical modelling of superelastic shape-memory alloys for seismic applications. Journal of Intelligent Material Systems and Structures 19 (1), 47–61.

Auricchio, F., Petrini, L., Pietrabissa, R., Sacco, E., 2003. Numerical modeling of shape-memory alloys in orthodontics. CMES – Computer Modeling in Engineering and Sciences 4 (3–4), 365–380.

Bernardini, D., Pence, T., 2005. Uniaxial modeling of multivariant shape-memory materials with internal sublooping using dissipation functions. Meccanica 40 (4), 339–364.

Bernardini, D., Rega, G., 2005. Thermomechanical modelling, nonlinear dynamics and chaos in shape memory oscillators. Mathematical and Computer Modelling of Dynamical Systems: Methods, Tools and Applications in Engineering and Related Sciences 11 (3), 291–314.

Bernardini, D., Rega, G., 2010. The influence of model parameters and of the thermomechanical coupling on the behaviour of shape memory devices. International Journal of Non-Linear Mechanics 45 (10), 933–946.

Bernardini, D., Vestroni, F., 2003. Non-isothermal oscillations of pseudoelastic devices. International Journal of Non-Linear Mechanics 38 (9), 1297–1313.

Bruno, O.P., Leo, P.H., Reitich, F., 1995. Free boundary conditions at austenite–martensite interfaces. Physical Review Letters 74 (5), 746–749.

Carreras, G., Casciati, F., Casciati, S., Isalgue, A., Marzi, A., Torra, V., 2011. Fatigue laboratory tests toward the design of SMA portico-braces. Smart Structures and Systems 7 (1), 41–57.

Collet, M., Foltête, E., Lexcellent, C., 2001. Analysis of the behaviour of a Shape Memory Alloy beam under dynamical loading. European Journal of Mechanics – A/Solids 20 (4), 615–630.

Delaey, L., Krishnan, R.V., Tas, H., Warlimon, H., 1974. Thermoelasticity, pseudoelasticity and memory effects associated with martensitic transformations. 1. Structural and microstructural changes associated with transformations. Journal of Materials Science 9 (9), 1521–1535.

Duerig, T., Pelton, A., Stöckel, D., 1999. An overview of nitinol medical applications. Materials Science and Engineering A, 149–160.

Feng, Z.C., Li, D.Z., 1996. Dynamics of a mechanical system with a shape memory alloy bar. Journal of Intelligent Material Systems and Structures 7 (4), 399–410.

Hartl, D.J., Lagoudas, D.C., Calkins, F.T., Mabe, J.H., 2010a. Use of a Ni60Ti shape memory alloy for active jet engine chevron application: I. Thermomechanical characterization. Smart Materials and Structures 19 (1), 015020.

Hartl, D.J., Mooney, J.T., Lagoudas, D.C., Calkins, F.T., Mabe, J.H., 2010b. Use of a Ni60Ti shape memory alloy for active jet engine chevron application: II. Experimentally validated numerical analysis. Smart Materials and Structures 19 (1), 015021.

He, Y.J., Sun, Q.P., 2010. Frequency-dependent temperature evolution in NiTi shape memory alloy under cyclic loading. Smart Materials and Structures 19 (11).

He, Y.J., Sun, Q.P., 2011. On non-monotonic rate dependence of stress hysteresis of superelastic shape memory alloy bars. International Journal of Solids and Structures 48 (11–12), 1688–1695.

Lacarbonara, W., Bernardini, D., Vestroni, F., 2004. Nonlinear thermomechanical oscillations of shape-memory devices. International Journal of Solids and Structures 41 (5–6), 1209–1234.

Lammering, R., Schmidt, I., 2001. Experimental investigations on the damping capacity of NiTi components. Smart Materials and Structures 10 (5), 853–859.

Leo, P.H., Shield, T.W., 1993. Transient heat transfer effects on the pseudoelastic behaviour of shape-memory wires. Acta metallurgica 41 (8), 2477–2485.

Li, D., Feng, Z., 1997. Dynamic properties of pseudoelastic shape memory alloys. In: International conference on Structural Dynamics: Recent Advances, No. 6, Southampton, UK.

Machado, L.G., Savi, M.A., Pacheco, P.M.C.L., 2003. Nonlinear dynamics and chaos in coupled shape memory oscillators. International Journal of Solids and Structures 40 (19), 5139–5156 (PACAM VII Special issue).

Masuda, A., Noori, M., 2002. Optimization of hysteretic characteristics of damping devices based on pseudoelastic shape memory alloys. International Journal of Non-linear Mechanics 37 (8), 1375–1386.

Meirovitch, L., 2001. Fundamentals of Vibrations.

Morin, C., Moumni, Z., Zaki, W., 2011. A constitutive model for shape memory alloys accounting for thermomechanical coupling. International Journal of Plasticity 27 (5), 748–767.

Ozbulut, O.E., Hurlebaus, S., 2011. Optimal design of superelastic-friction base isolators for seismic protection of highway bridges against near-field earthquakes. Earthquake Engineering and Structural Dynamics 40 (3), 273–291.

Piedboeuf, M.C., Gauvin, R., Thomas, M., 1998. Damping behaviour of shape memory alloys: strain amplitude, frequency and temperature effects. Journal of Sound and Vibration 214 (5), 885–901.

Predki, W., Klönne, M., Knopik, A., 2006. Cyclic torsional loading of pseudoelastic NiTi shape memory alloys: damping and fatigue failure. Materials Science and Engineering: A 417 (1–2), 182–189.

Saadat, S., Salichs, J., Noori, M., Hou, Z., Davoodi, H., Bar-On, I., Suzuki, Y., Masuda, A., 2002. An overview of vibration and seismic applications of NiTi shape memory alloy. Smart Materials and Structures 11 (2), 218–229.

Seelecke, S., 2002. Modeling the dynamic behaviour of shape memory alloys. International Journal of Non-Linear Mechanics 37 (8), 1363–1374.

Shaw, J.A., Kyriakides, S., 1995. Thermomechanical aspects of NiTi. Journal of the Mechanics and Physics of Solids 43 (8), 1243–1281.

Sun, Q.P., Hwang, K.C., 1993. Micromechanics modelling for the constitutive behaviour of polycrystalline shape memory alloys – I. Derivation of general relations. Journal of the Mechanics and Physics of Solids 41 (1), 1–17.

Zhang, X., Feng, P., He, Y.J., Yu, T., Sun, Q.P., 2010. Experimental study on rate dependence of macroscopic domain and stress hysteresis in NiTi shape memory alloy strips. International Journal of Mechanical Sciences 52 (12), 1660–1670.